Journal of Nuclear Materials 406 (2010) 127–137

Contents lists available at ScienceDirect

Journal of Nuclear Materials

journal homepage: www.elsevier.com/locate/jnucmat

The effect of prior cold-work on the deformation behaviour of neutron irradiated AISI 304 austenitic stainless steel

Wade Karlsen [a,*], Steven Van Dyck [b]

[a] VTT Technical Research Centre of Finland, P.O. Box 1000, FI-2044 VTT, Finland
[b] TCH, SCK-CEN, Boeretang 200, Mol B-2400, Belgium

A B S T R A C T

Cold-work is intentionally employed to increase the yield strength of austenitic stainless steels and also occurs during fabrication processes, but it has also been associated with greater incidence of stress corrosion cracking. This study examined the effect of up to 3.85 dpa neutron irradiation on the deformation behaviour and microstructures of 30% cold-worked AISI 304 material tensile tested at 300 °C. While the deformation behaviour of 0.07 dpa material was similar to non-irradiated material tested at the same temperature, its stress–strain curve was shifted upwards by about 200 MPa. Materials irradiated to over 2 dpa hardened some 400–500 MPa, but showed limited strain hardening capacity, exhibiting precipitous softening with further straining beyond the yield point. The observed behaviour is most likely a consequence of planar deformation products serving as strengtheners to the unirradiated bulk on the one hand, while promoting strain localization on the other, behaviour exacerbated by the subsequent neutron irradiation.

1. Introduction

As the world's fleet of light-water reactor (LWR) nuclear power plants age, cracks have emerged in stainless steel structural components exposed to neutron irradiation. The fractures often exhibit a characteristic intergranular-type crack propagation path, and are classified as irradiation-assisted stress corrosion cracking (IASCC). The ability to predict the instances and extent of such cracking would enable better assessment of the performance and integrity of reactor structural components, for safe extension of the operating lifetime of power plants. The phenomenon of IASCC is dependent upon mechanical, material, and electrochemical issues, each of which itself involves many interdependent variables which can act in synergistic manners to induce the observed fracture along grain boundaries. IASCC-focused research has classically been corrosion-weighted, often being treated as a subset of intergranular stress corrosion cracking (IGSCC). However, as early as in 1989, a transition from transgranular (TG) to intergranular (IG) fracture was reported for a ~7 dpa irradiated stainless steel during slow strain rate testing (SSRT) in 300 °C *argon*, a non-corrosive, inert environment [1]. More recently, other researchers have *also* reported intergranular fracture in independently-conducted SSRT experiments in pure argon, in 1.7 dpa sensitized 304 stainless steel [2] and 30 dpa non-sensitized 304 stainless steel [3]. Further, in non-irradiated materials, *cold-work* has been linked to accelerated cracking in otherwise resistant materials [4]. That demonstrates the critical importance of understanding the contribution of purely-mechanical factors to the intergranular cracking often considered to be IASCC. In particular, in cases where cold-working has been employed in order to increase the strength and hardness of a material for particular applications (e.g. baffle bolts), or where cold-work has occurred during fabrication (weld-shrinkage, surface machining), the effect of subsequent neutron irradiation on the mechanical performance of the cold-worked material is of interest.

The effect of irradiation on the tensile behaviour of austenitic stainless steels has been studied for many years. The yield strength of 300-series austenitic stainless steels increases with increasing irradiation dose, going from less than 200 MPa in the non-irradiated, annealed condition, to levels in the 800–1000 MPa range at doses above about 1 dpa [5]. Above about 1 dpa initial yielding is followed by a drop in the measured engineering stress. With increasing dose the ductility decreases, and in many cases the fracture toughness decreases as well. The effect of irradiation is also temperature dependent [6]. Irradiation hardening has a maximum effect when irradiation and mechanical testing are conducted at ~300 °C, with the post-irradiation strength decreasing weakly with temperature below 300 °C, and relatively rapidly with increasing temperature *above* 300 °C. The *uniform* tensile elongation, meanwhile, is minimized at 300 °C but increases above or below that point [6]. The primary issue is a very low (⩽1%) strain to necking in materials irradiated to a dose of several displacements per atom (dpa), and thus a high level of localized plasticity. However, the

* Corresponding author. Tel.: +358 20 722 6865; fax: +358 20 722 7002.
E-mail address: wade.karlsen@vtt.fi (W. Karlsen).

0022-3115/$ - see front matter © 2010 Elsevier B.V. All rights reserved.
doi:10.1016/j.jnucmat.2010.01.028

literature regarding the effect of cold-work prior to irradiation on the subsequent deformation behaviour at LWR temperatures is sparse [7]. Nonetheless, the neutron irradiation has been reported to modify the dislocation structure introduced by cold-working. That results in retardation of the development of irradiation defects in the material, and thus also in the evolution of the mechanical properties with increasing dose. The irradiation-induced shift in the properties may therefore be somewhat smaller, while the resulting yield stress of initially cold-worked materials may be somewhat higher after irradiation when compared to that in initially annealed material [8].

Underlying the observed mechanical behaviour of stainless steels are the deformation mechanisms in operation. The deformation mechanisms possible within the face-centred cubic (fcc) lattice of austenitic materials are particularly diverse, but they all tend to occur most readily at the close-packed cube-diagonal of the lattice (i.e. on the {1 1 1} planes). In low stacking fault energy (SFE) austenitic stainless steels in particular, the lower SFE allows broad separation of the partial dislocations, with a stacking fault between them. This not only restricts cross-slip, but the formation of stacking faults on every other close-packed plane can in fact produce hexagonally-close packed (hcp) epsilon martensite [9]. Additionally, a twin can be produced by the glide of Shockley partial dislocations of the same sign on *successive* {1 1 1} planes [10].

The most significant factor for *irradiated* stainless steel deformation is the presence of irradiation-induced obstacles that increase the stress level needed to activate dislocation glide. As has been well described elsewhere, such defects primarily consist of dislocation loops and defect clusters, the population and size of which increase rapidly up to 1 dpa of dose, thereafter primarily growing only in size but not in quantity. Peculiar to irradiated materials is also a very important deformation mechanism referred to as dislocation channel deformation (DCD). In the classical sense, dislocation channelling is a process of heterogeneous plastic deformation by ordinary dislocations, in which dislocations released from a source glide along the limited slip planes within the band, removing or cutting through small barriers in their paths [11]. The defect-clearing process then produces an easy path for subsequent dislocation glide. When viewed edge-on in a thin foil, such a region appears as a narrow, clear channel on the order of 50–200 nm in width [10]. But in the bulk material it is in fact a thin slab of softer material, constrained on its edges by the grain boundaries, and above and below it by the defect hardened matrix. This preferential path for dislocation motion results in strain localization, which produces intense shear bands that emerge at the specimen surface. The onset of DCD is thought to be responsible for the localized necking and sharp reduction in uniform elongation observed at higher doses.

The purpose of this study was to examine the deformation behaviour and mechanisms of a cold-worked austenitic stainless steel following neutron irradiation.

2. Experimental

The material of this study was a type AISI 304 austenitic stainless steel rod in the 30% cold-drawn condition. It had the composition (in wt.%) of Fe with 18.4 Cr, 8.5 Ni, 1.56 Mn, 0.33 Si, 0.02 S, and 0.04 C. The material was homogeneous and had a uniform grain structure with an average size of 15 μm in the cross section. In the longitudinal section the grains were elongated in the rod's axial direction, with an average aspect ratio of 1.4 (i.e. 19 μm in axial and 14 μm in radial directions). In addition to a fine average grain size, the cold-working had induced an abundance of closely-spaced mechanical twins in the microstructure.

Table 1
The irradiated materials and tensile test matrix of this study.

ID	Dose (dpa)	Test temperature (°C)	Test description	TEM
Ref1	0	25	Tensile test to failure	X
Ref2	0	300	Tensile test to failure	X
X0	0.07	300	Tensile test to failure	X
X5	2.21	300	Tensile test to failure	
Y4	2.44	300	Test interrupted *after* peak stress	X
Y3	2.49	300	Test interrupted *before* peak stress	X
Y2	2.49	300	Tensile test to failure	
Y0	3.85	300	Tensile test to failure	X

The material was irradiated in the BR2 reactor to a range of doses, shown in Table 1. The irradiation was carried out in flowing water at 300 °C and 15 MPa pressure. The water chemistry was representative of PWR primary water, containing 400 ppm boron as boric acid and 2.1 ppm lithium as lithium hydroxide. Hydrogen was added to the water to a level of 30 cc/kg (referred to standard temperature and pressure). The maximum fast flux in the irradiation channel was 8×10^{13} n/cm^2 s ($E > 1$ MeV) and the variation in position (for all samples in Table 1 except Y0) and irradiation time (Y0 was irradiated longer) gave rise to the range of doses on the different samples. The damage doses in Table 1 have been determined based on the proportionality between fluence and dpa: 10^{21} n/cm^2 ($E > 1$ MeV) being equivalent to 1.5 dpa for an LWR representative spectrum. The original 6 mm diameter rod was machined into round tensile test specimens having a gauge region 3 mm diameter and 10 mm long. The materials were then slow strain rate tensile (SSRT) tested using a stepper-motor test rig at a crosshead speed of 0.2 mm/min, without the use of a strain gauge. While most of the tests were conducted all the way through failure, specimens Y3 (2.49 dpa) and Y4 (2.44 dpa) were subjected to interrupted tests. Specimen Y4 was interrupted at a strain level exceeding the initial yield peak, while specimen Y3 was interrupted at a point *preceding* the expected yield peak.

Transmission electron microscopy (TEM) was carried out on the as-received cold-worked material, and on selected materials following the tensile testing. In tests to fracture the specimens were extracted from close to the fracture surface of one of the bar halves, while in the two interrupted tests, the blanks for TEM foil production were extracted from the middle of the gauge region.

TEM specimen preparation was carried out in a semi-hot-cell facilities beginning with thin discs that had been dry-sawn from the test-bars perpendicular to the bar axis. The discs were deburred and further ground on both sides using 1200 grit SiC grinding papers, until a thickness of 0.06 mm was achieved. The discs were then thinned to electron transparency with a Tenupol Twin-jet electropolisher, using a solution of 5% perchloric acid in acetic acid at 25 °C and +70 V. TEM observations were made using a Philips CM200 field emission gun TEM operating at 200 kV. The reciprocal lattice rod technique was employed for imaging the irradiation-induced loop population of the least-deformed material, Y3 (2.49 dpa), as described in [12].

3. Results

3.1. Mechanical tests

The engineering mechanical properties calculated from the load–displacement data generated by the tensile tests are shown in Table 2. All of the irradiated materials except the lowest dose X0 (0.07 dpa) one behaved in a very similar manner, producing very similar tensile properties. Fig. 1 shows the stress–strain behaviour calculated from the load–displacement data for the

Table 2
Calculated engineering tensile properties for round specimens of cold-worked 304 rod material in non-irradiated and irradiated conditions.

ID	Dose (dpa)	Test temperature (°C)	Yield strength (MPa)	Ultimate tensile strength (MPa)	Uniform elongation (%)	Total elongation (%)
Ref1	0	25	710	845	25	50
Ref2	0	300	605	656	6	21
X0	0.07	300	735	798	8	23
X5	2.21	300	957	974	1	15
Y2	2.49	300	979	995	0	15
Y0	3.85	300	1020	1034	0	14

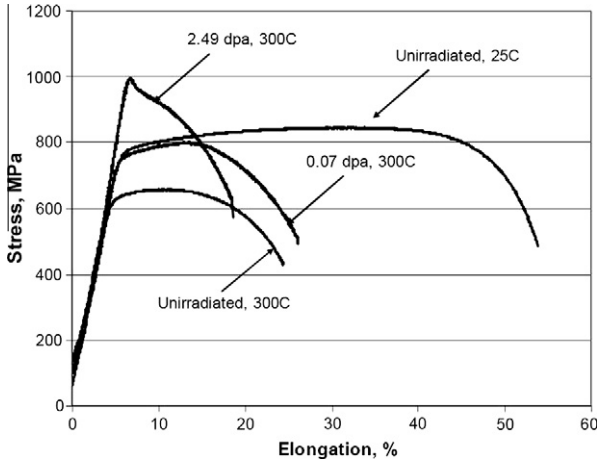

Fig. 1. Engineering stress–strain plot comparing the tensile behaviour of the 304 stainless steel of this study, which was first cold-worked and subsequently irradiated to different levels.

non-irradiated materials and selected irradiated materials. The curves are normalized to one another by shifting them along the X-axis, since the different test machines used for the non-irradiated and irradiated materials had different degrees of rigidity in their mechanisms. Fig. 2 shows the locations of the stress–displacement curve at which the tests were interrupted for Y3 and Y4 (2.49 and 2.44 dpa, respectively).

As shown in the curves, although substantially hardened, the non-irradiated, cold-worked material still has significant hardening capacity remaining, and exhibited marked ductility, especially

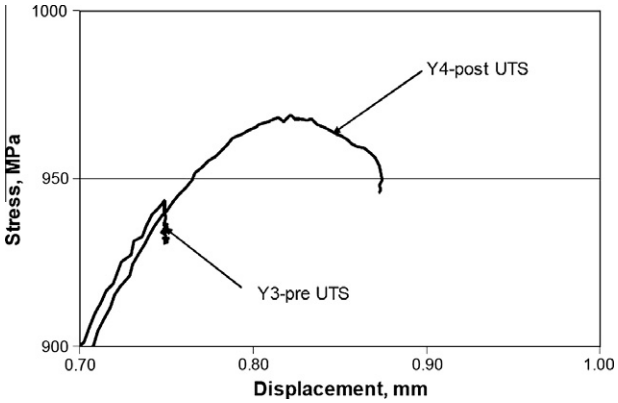

Fig. 2. Engineering stress-displacement curve for tensile bars Y3 (2.49 dpa) and Y4 (2.44 dpa), tested at 300 °C and a strain rate of 3×10^{-4} s, and interrupted just before and just after the UTS, respectively.

when tested at room temperature. A comparison between the tensile behaviour of the irradiated and non-irradiated materials at 300 °C shows that the 0.07 dpa irradiated material was similar in form to that of the non-irradiated material tested at the same temperature, but the irradiated material's stress–strain curve was shifted upwards by about 200 MPa with respect to the non-irradiated material and exhibited similar or even slightly greater elongation. The materials irradiated to greater levels, however, all showed similar behaviour as that of the example shown in the figure. Although neutron irradiation hardened them an additional 200–300 MPa over that of the 0.07 dpa material, they all showed an extremely limited capacity for additional work hardening, mostly exhibiting continuous softening with further straining beyond the yield point. Nonetheless, SEM examinations of the fracture surfaces following testing showed ductile dimple type fracture in all cases, including for the highest dose materials.

3.2. Results of TEM examinations

3.2.1. Non-irradiated materials

TEM examination of the untested cold-worked material revealed a very heterogeneous distribution of deformation features in the microstructure. All of the principle face-centred-cubic deformation mechanisms were present in the material, generally co-existing to varying degrees in different regions of a given specimen. A high density of dislocations tended to form specifically-oriented bands with more random, sparser tangles between them. On the other hand, there were also regions of the specimen dominated by twins. Fig. 3 shows the bright field and dark field view of the twinned structure, in which the twin plane is shown to be the {1 1 1} type plane. The streaks visible in the diffraction pattern are a consequence of simultaneous contribution from the many finely-spaced micro-twins. Although in many ways similar in outward appearance to micro-twins, the existence of transgranular bands of deformation-induced epsilon martensite in the microstructure were distinguished separately from the twins, based on their diffraction pattern, as shown in Fig. 4. The diffraction pattern shown is composed of strong double-diffraction spots of the epsilon phase, as a consequence of the asymmetrical orientation of the {1 1 1}-type gamma iron planes in that particular specimen orientation near the ⟨1 2 3⟩-type zone axis. Although epsilon martensite-type stacking of planes may be achieved with only a few planes, thicker regions constructed of many more planes diffract much more strongly, consequently appearing much brighter in the dark-field image. Further deformation during tensile testing at either room temperature or elevated temperature seemed to mostly lead to increased amounts of the deformation features already observed in the cold-worked material, particularly twins, with small twins occurring between larger twins. As shown in Fig. 5, it was also possible to detect alpha martensite at the intersection of twins, particularly in the room temperature test specimen.

3.2.2. Irradiated materials

The reciprocal lattice rod technique was employed for imaging the irradiation-induced loop population of the least-deformed material, Y3 (2.49 dpa), as shown in Fig. 6. The result showed an apparent loop density of 3×10^{23} m^3, having an asymmetrical size distribution as shown in Fig. 7. A mean loop diameter of 4 nm was calculated for the material. Separate loop quantification was not made for the Y4 (2.44 dpa) material, as its dose was so similar to that of Y3. The rel-rod technique was not possible for the X0 material, as the dose (0.07 dpa) was too low for adequate imaging of faulted loops.

General observations made of the deformed irradiated materials at relatively low magnifications revealed a heavily distorted

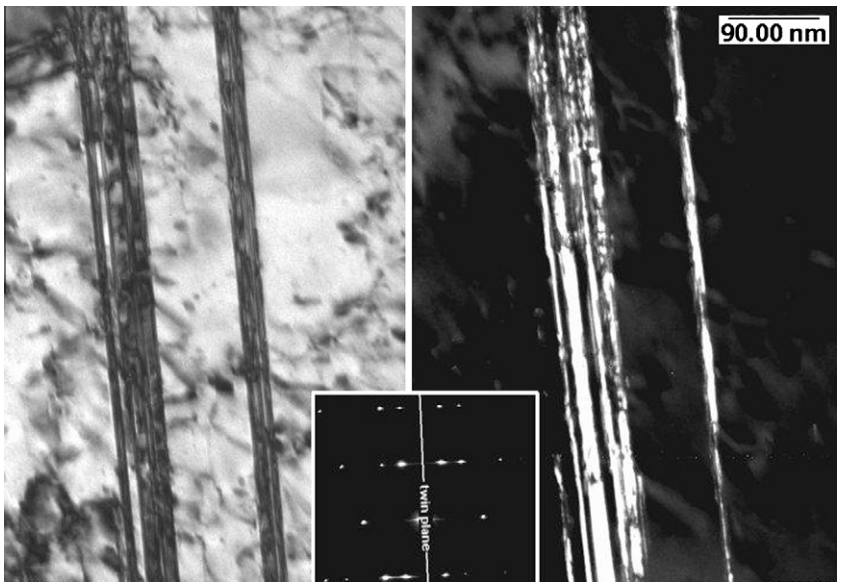

Fig. 3. Fine twins in the as-received, non-irradiated, cold-worked 304 material, shown in bright field (left) and dark field (right) conditions. The diffraction pattern, near the ⟨1 1 0⟩-type zone axis, shows the orientation of the {1 1 1}-type twin plane with respect to the images. The streaks in the diffraction pattern perpendicular to the twin plane are a consequence of multiple small, parallel twins being present in the same selected area.

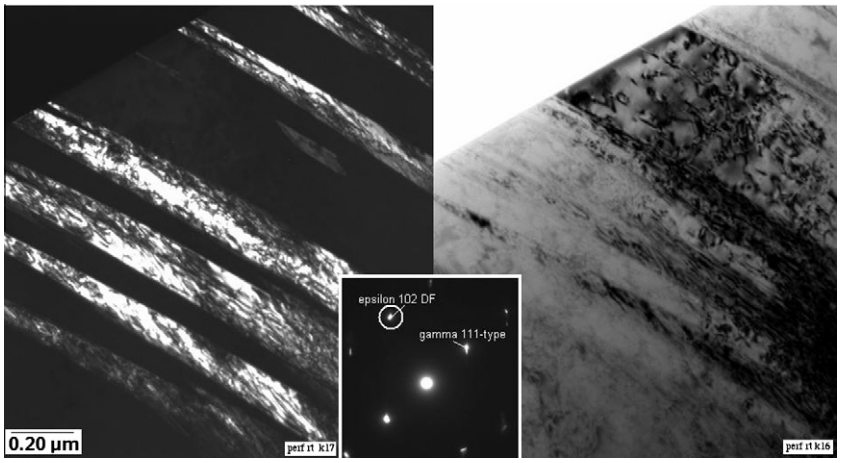

Fig. 4. Epsilon martensite in the as-received, non-irradiated, cold-worked 304 material, shown in bright field (left) and dark field (right) conditions. The diffraction pattern includes double-diffraction of the epsilon phase ⟨1 0 2⟩-type spot as a consequence of the asymmetrical orientation of the {1 1 1}-type gamma iron planes in that particular specimen orientation.

microstructure in all cases. All of the materials also exhibited some population of bands, which appeared either dark or light. As shown in Fig. 8, tilting the foil to various degrees induced contrast alterations, such that a dark band in a light surrounding became a light band in a dark surrounding. A comparison of the more mildly-irradiated but more highly-strained X0 material with the more highly-irradiated and significantly strained Y4 material revealed two important differences: the irradiation-induced defect population of the X0 material was less significant in size and density than that of the Y4 material and the X0 material still had a significant population of linear dislocations remaining, while in the Y4 material the irradiation had replaced the linear dislocation population with defects (Figs. 9 and 10). Comparing the less strained Y3 material with the more strained Y4 material of similar irradiation level suggested that the Y4 material may have a greater population of bands than the Y3 material, Fig. 11. The bands in the more highly strained Y4 material also appeared to be sharper-edged and narrower than the broader, more diffuse bands of Y3. Like that of the Y4 material, the bands of the more significantly-strained X0 material *also* seem narrow and sharp-edged, Fig. 12. The apparent width and spacing of the bands varied significantly from grain to grain for a given material though, as shown for Y4 in Fig. 13.

Of particular interest was identification of the true nature of the bands observed in the irradiated materials. To explore their character, selected-area diffraction (SAD) analyses were carried out in regions tilted to the [1 1 0] zone axis. The bands exhibited a variety of diffraction behaviours in that orientation. In some cases they seemed to show twin character, generating distinct twin spots at the 1 1 0 zone axis. In other orientations though, bands that had been visible as light bands near the 1 1 0 zone axis, induced only a slight alteration of the diffraction pattern at the 1 1 0 zone axis, albeit to such an extent that clear satellite spots were produced in the diffraction pattern. Yet other such bands exhibited *no* extra spots in the corresponding diffraction patterns, suggesting no

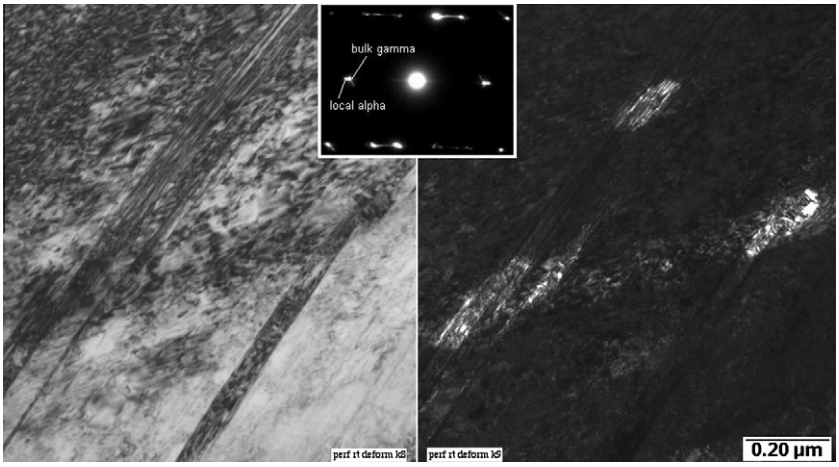

Fig. 5. Alpha martensite at the intersection of micro-twins in the non-irradiated, cold-worked 304 material following room temperature deformation, shown in bright field (left) and dark field (right) conditions. The dark-field image is composed only of the alpha portion of the two closely-spaced alpha- and gamma iron spots indicated in the diffraction pattern.

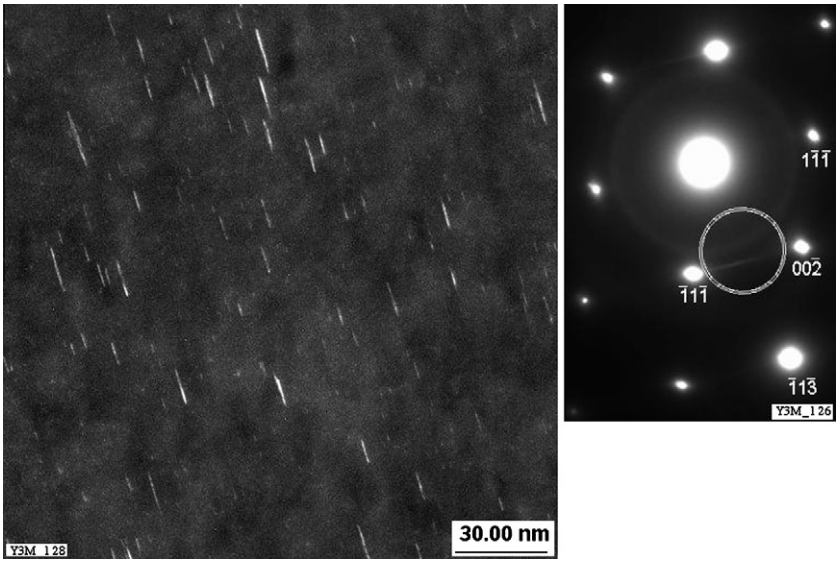

Fig. 6. A reciprocal lattice rod image of the faulted loops in the 2.49 dpa Y3 material, using the conditions shown in the accompanying selected-area diffraction (SAD) pattern, and the circled rel-rod streak. In this orientation one of four variants is visible.

difference in lattice orientation in that position. Taken as a whole though, there seemed to be no obvious, consistent orientation relation between the matrix and the bands that would allow them to be definitively identified as e.g. always traditional austenite deformation twins or always bands of epsilon martensite. As shown in Fig. 14, a dark-field image composed with the 1 1 1-type austenite spot revealed that the grey bands running from bottom to top in the image were apparently cleared of irradiation defects. The intersection of those bands with the more stark bands oriented horizontally in the image, caused the latter bands to be cut, and perhaps even shifted. It would seem, therefore, that the long, grey bands in that image correspond to the defect-free "channels" described in the literature. When strain is localized in such channels, they reportedly cause steps in features they intersect. A similar phenomenon was observed in the X0 material, as was shown already in Fig. 10. Creating a dark-field image with one of the additional spots produced by the band itself, revealed what were apparently ribbons of stacking faults along the length of the band, Fig. 15. On the other hand, equally close examination of the twins of Fig. 16 does not enable such ready distinction of a stacking fault population, though the contrast is also patchy like that of the previously-described bands. In both cases the imaging took place at

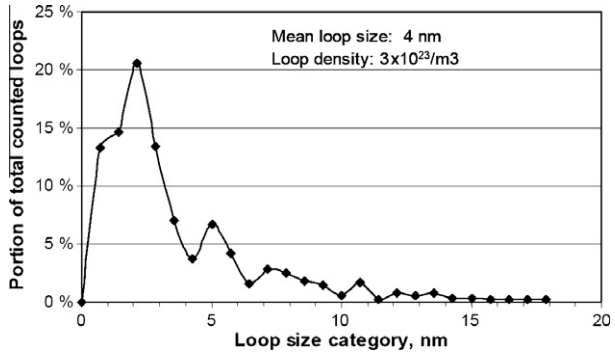

Fig. 7. The distribution of the faulted loop population of Y3. The resolution of the images was limited, so the actual number of counts around the 1 nm loop diameter range is less accurate.

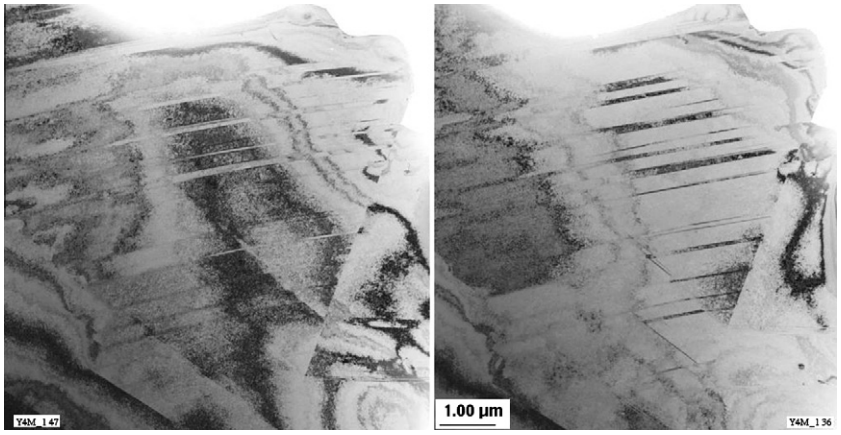

Fig. 8. The typical appearance of some bands in one region of Y4, imaged at two different tilt angles. The bands which appeared light in the left-hand image appear dark in the right-hand image.

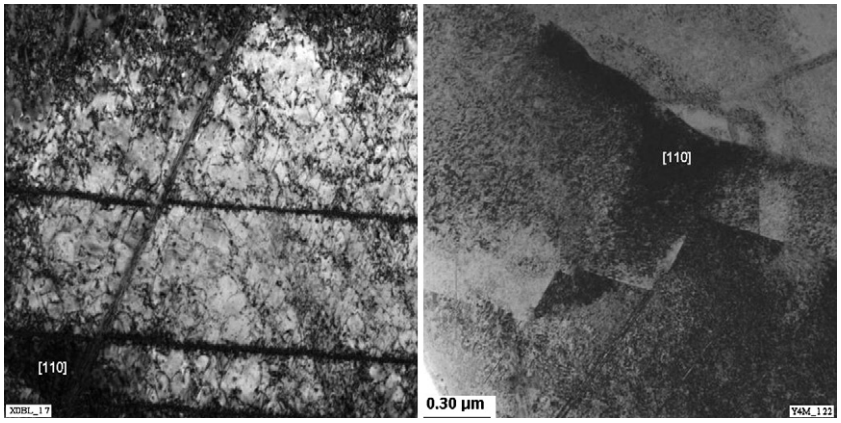

Fig. 9. The microstructures of 0.07 dpa X0 (left) and 2.44 dpa Y4, viewed near 1 1 0 zone axes and at the *same* magnification. Linear dislocations populate X0 throughout, while Y4 mostly exhibits the fine-textured contrast typical of irradiated microstructures. Some thin bands are visible in both cases, while the geometrical boundary in Y4 also suggests a twinned microstructure.

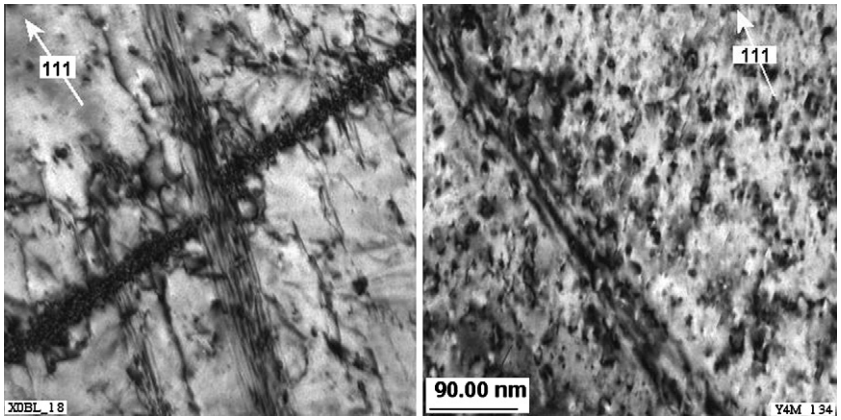

Fig. 10. The microstructures of X0 (left) and Y4 at the same high magnification. The population of irradiation defects in Y4 is more obvious at this magnification. Both materials show some bands. The intersection of one band in X0 appears to create a step in the other one.

the ⟨1 1 0⟩ zone axis. Closer inspection was also made of the bands shown earlier in though, which were tilted away from the ⟨1 1 0⟩ zone axis. They exhibited what could best be described as incomplete bands, as shown in Fig. 17, while a dark-field image from the same specimen area, shown in Fig. 18, also includes what are likely the faults of dislocation loops existing in the "incomplete area" between the bright regions.

4. Discussion

The results indicated a clear effect of irradiation in altering the deformation behaviour of the cold-worked material. Fig. 19 shows a comparison between the deformation behaviour of the cold-worked material of this study and an annealed material from another study [13], in both the non-irradiated and mildly-irradiated

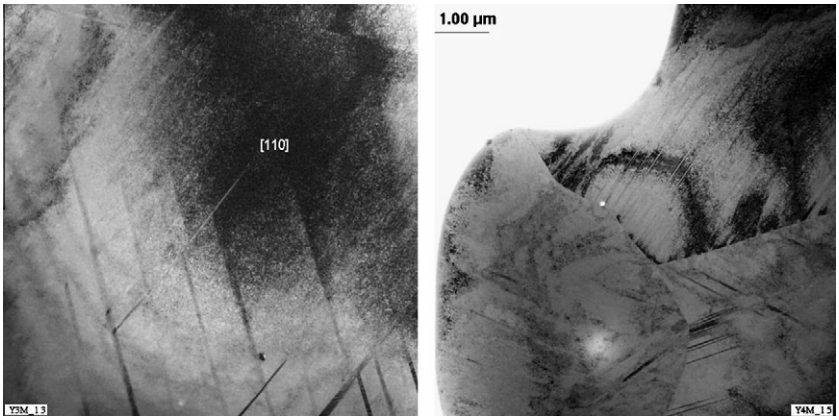

Fig. 11. General microstructures of the less strained 2.49 dpa Y3 (left) and the morestrained 2.44 dpa Y4 materials at the same magnification. Both have bands, but most of the ones in Y3 seem broader and more diffuse than the ones in Y4, with the exception of the narrow, bright band in the [1 1 0] zone of Y3.

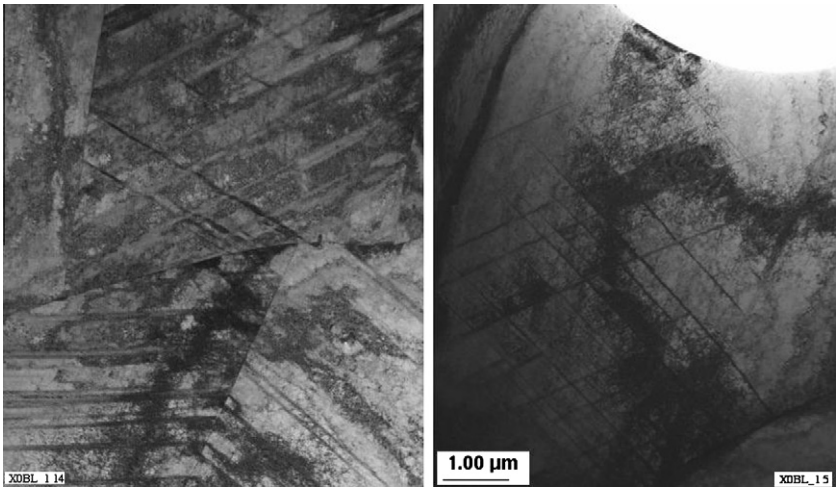

Fig. 12. More examples of the banded microstructure of the strained-to-fracture 0.07 dpa X0, which suggest that there may be overall more of the narrow bands present in the more extensively strained X0 material than in the more highly irradiated, but *less* strained Y3 and Y4 specimens.

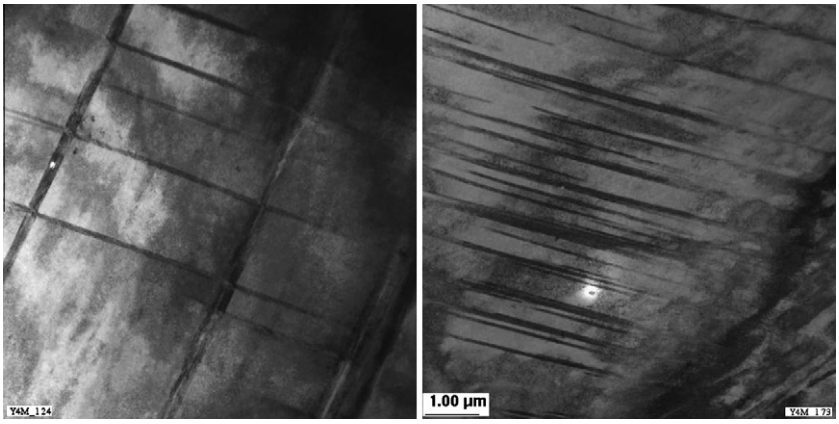

Fig. 13. General microstructures of Y4 at same magnification, but showing the range in the frequency of the band population in different regions of the foil.

conditions, for similar dose, carbon content and test temperature. In both cases irradiation increased the yield and ultimate tensile strengths. Nonetheless, while the increase in yield strength due to irradiation was 130 and 200 MPa for the cold-worked and the annealed materials respectively, in the unirradiated condition the cold-worked material had a yield strength that was over 500 MPa greater than that of the annealed material of the reference study. Thus, the strengthening effect of the cold-work was far greater than that of the irradiation at the low dose. A similar observation can be made with regards to the strain hardening behaviour. While all of the curves in Fig. 19 exhibit strain hardening, the unirradiated annealed material strain hardened by about 360 MPa,

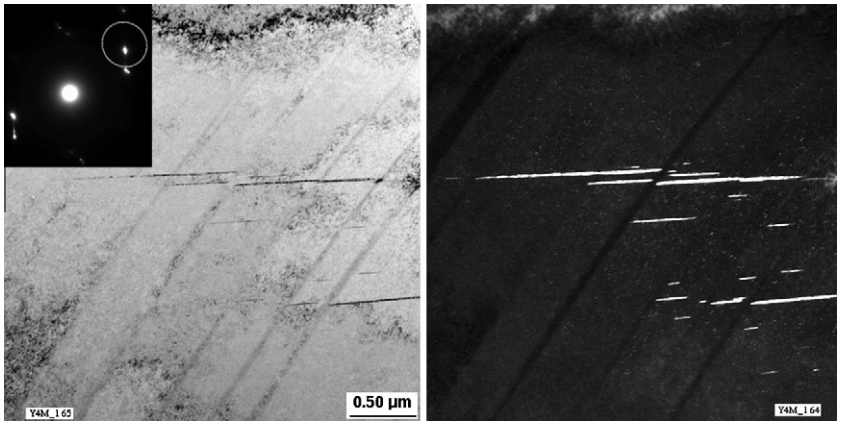

Fig. 14. A bright field (left) and corresponding dark-field image composed utilizing the circled spot in the SAD. The small bright dots in the DF image are due to radiation defects. It would appear that the bands have been swept of such defects.

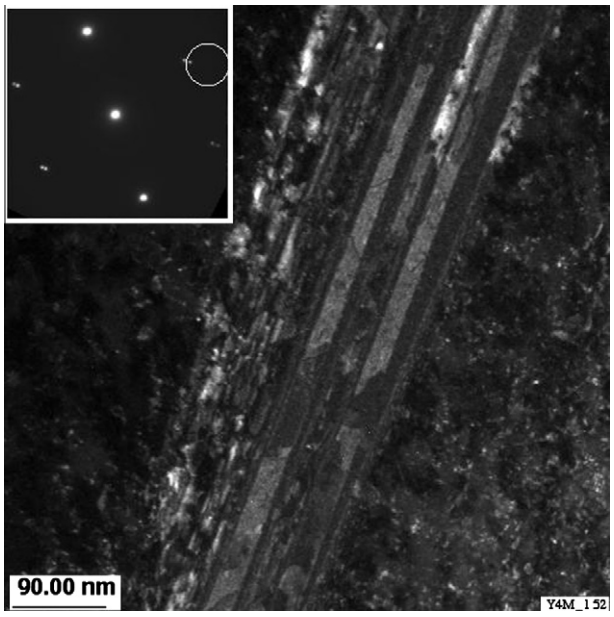

Fig. 15. Closer examination of stacking faults within a channel in Y4, imaged in dark field using the extra spot near the matrix 1 1 1-type spot.

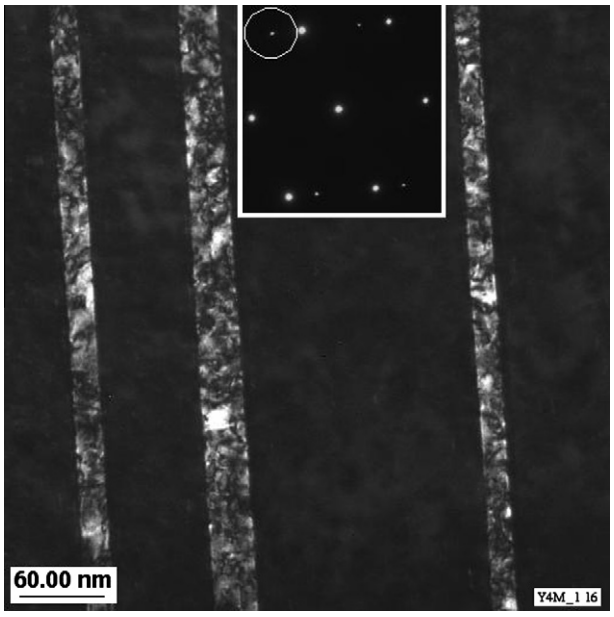

Fig. 16. Closer examination of *twin* bands in Y4, imaged in dark field using the twin spot indicated.

while the unirradiated cold-worked material strain hardened by only 51 MPa. The annealed material of the reference study never reached the strength level that the cold-worked material exhibited though. The irradiated annealed material showed less strain hardening capacity and total elongation than in the unirradiated condition, but it still hardened by an additional 218 MPa. However, at a similar level of irradiation the cold-worked material actually exhibited slightly greater strain hardening capacity and total elongation than its non-irradiated counterpart, hardening by 63 MPa (though that was still less than exhibited by the annealed material.) What the comparisons in Fig. 19 shows overall though, is the fact that, at the lower dose level, the strengthening by strain hardening is at least as significant as the increase in strength occurring as a consequence of irradiation.

At higher dose levels, a yield peak is typically observed and strain hardening is suppressed. Such behaviour was also observed for the higher dose materials of the current study that were cold-worked prior to irradiation. Fig. 20 shows a comparison between the deformation behaviour of the higher dose cold-worked material of this study and a high dose *annealed* 304L material from another study [14], for a similar test temperature. While a yield peak is evident in both cases, the yield strength of the cold-worked and irradiated material was about 400 MPa higher than that of the material irradiated in the annealed condition. However, a comparison of the yield strength of the high dose annealed material to that of the non-irradiated annealed material of Fig. 19 shows a yield strength of at least about 450 MPa higher for the more heavily-irradiated material. Likewise, the yield strength of the cold-worked material was about 400 MPa higher when irradiated to 3.85 dpa, which is similar in magnitude to the effect of cold-work alone. On the other hand, while the cold-worked material continuously softened immediately following the yield peak, the annealed material showed a significant delay before the onset of further softening. That indicates that the prior cold-work had a significant impact on the subsequent deformation behaviour of the irradiated material.

Underlying the deformation behaviour are the deformation mechanisms. The principle deformation mechanisms observed to

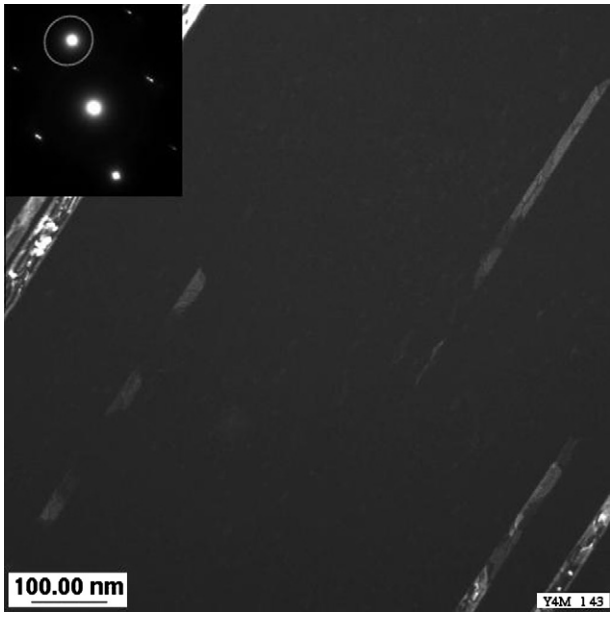

Fig. 17. Tilted away from [1 1 0], these bands in another region of Y4 are in contrast. The DF image was composed using the indicated spot.

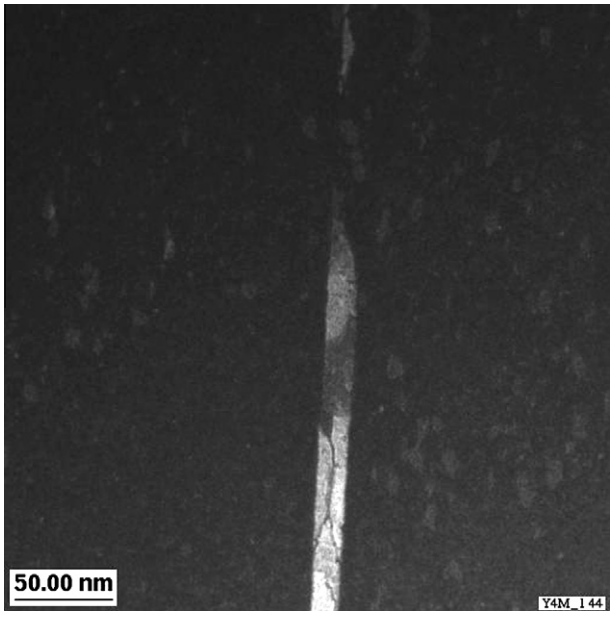

Fig. 18. Closer view of an evolving band from the same region as Fig. 17.

be in operation in the cold-worked, non-irradiated 304 stainless steel were similar to those described by Hashimoto et al. for 304 and 316-type stainless steels [15]. In other words, there were already dense dislocation tangles, along with deformation-induced twins, epsilon martensite, and alpha martensite present in the cold-worked condition. These features all promote strain hardening because they interrupt the glide planes of dislocation in the same manner as grain boundaries do, which then increases the incidences of dislocation pile-ups. When viewed in a thin foil, the twins and epsilon martensite appeared as bands within the microstructure, but because they possess a sufficiently different lattice structure, they diffracted differently in the TEM, leading to contrast differences. The irradiated materials *also* showed such bands, but in particular the higher dose materials did not strain harden,

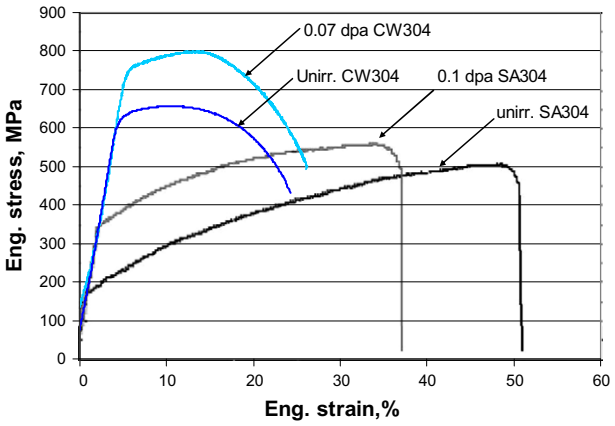

Fig. 19. Comparison between the deformation behaviour of the cold-worked material of this study and an annealed material of similar carbon content from another study [13], in both the non-irradiated and mildly-irradiated conditions, at similar dose and test temperature.

behaviour which is associated with dislocation channels. Recent work on 304 stainless steel material has shown that, even at a dose as low as 0.10 dpa, channel deformation occurs at least in early stages of deformation [16]. But as described in that reference, there is a propensity for slip to occur in 304 by partial dislocations, which then rapidly populates the channels with stacking faults, epsilon martensite, and ultimately twin-type planar stacking. Thus, even though the deformation structures in the irradiated cold-worked materials are similar in appearance to those in the non-irradiated cold-worked material, it is likely that the bands are still a symptom of channel deformation.

The presence of bands in both non-irradiated and irradiated deformed materials is a symptom of non-heterogeneous deformation. Whether irradiated or not, segregation of partial dislocation motion to particular planes in a material can lead to bands of strained material, which is a form of strain localization. The effect of irradiation is simply to maintain the deformation localization with increasing stress, by presenting a greater obstacle to dislocation glide outside the channel. That was demonstrated in this material by the fact that in the 0.07 dpa X0 material dislocations were also present outside of the bands, whereas in the more highly-irradiated and also significantly strained 2.44 dpa Y4 material, they were not. This is despite the fact that the stress in Y4 rose as high as about 970 MPa, whereas the maximum stress achieved in the X0 material was only about 800 MPa.

The cold-work prior to irradiation, meanwhile, played several different roles. On the one hand, it was observed that the dislocations induced during the cold-work had effectively been erased during the course of the subsequent irradiation. As has been described elsewhere [7,17], prior cold-work can slow the evolution of the irradiation-induced dislocation loop structure, most likely as a consequence of the linear dislocations serving as sinks for the point defects produced during irradiation. As shown in Fig. 21, the 2.49 dpa material of this study had a similar dislocation loop density as the annealed materials of the reference study, but the average loop diameter was very much lower for the same level of irradiation. That retardation of the defect development could explain why the 0.07 dpa material did not suffer as much loss of strain hardening capacity as the 0.1 dpa annealed material shown previously in Fig. 19.

On the other hand, as mentioned earlier, the extensive twinning and epsilon bands in the microstructure following cold-work effectively reduce the grain size of the material. Even following irradiation, these boundaries could be expected to remain in the

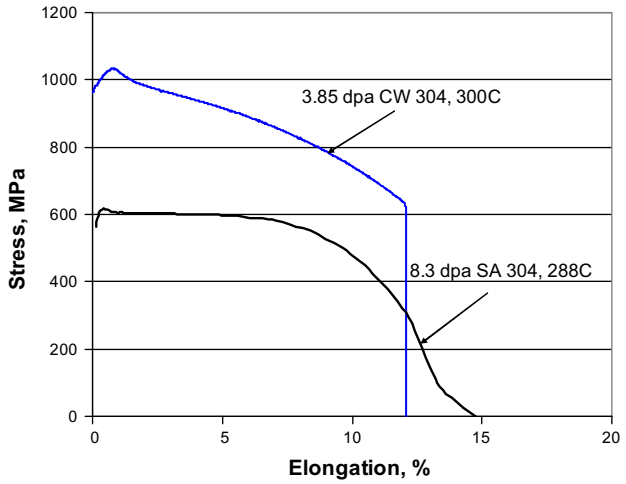

Fig. 20. Comparison between the deformation behaviour of the cold-worked material of this study and a neutron-irradiated annealed material from another study [14], at similar test temperature and for irradiation levels exceeding the dose at which the loop density is considered to be saturated.

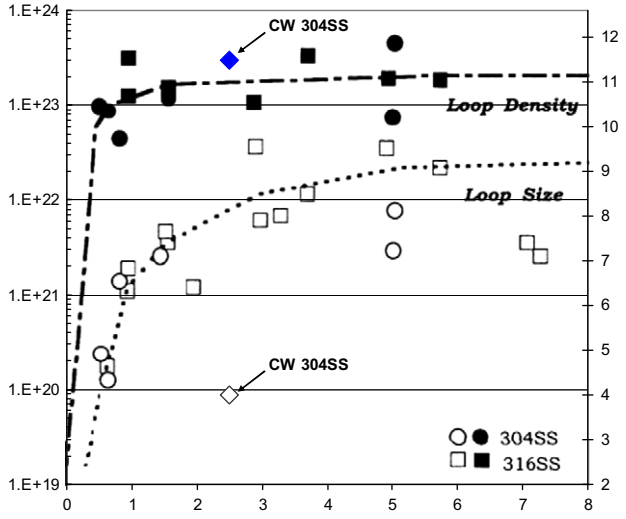

Fig. 21. The loop density and loop diameter of the 2.49 dpa Y3 material of this study, overlaid on data from Bruemmer et al. [5].

microstructure, as was evident in Fig. 11. The dislocations gliding within the channels must therefore still interact with those boundaries, as has been described by Edwards et al. in studies of irradiated copper [18]. Thus, since the cold-worked material's yield strength is still higher in the non-irradiated condition than that of an annealed material irradiated even to 8 dpa (Fig. 20), it seems likely that the strengthening of the *irradiated* cold-worked material is probably still principally a function of the cold-work deformation products, rather than of the dislocation loop population. Likewise, since softening is a consequence of strain localization, it seems likely that the immediate onset of strain softening in the higher dose cold-worked materials is primarily a consequence of the fact that the yield strength is already quite high, so strain immediately localizes to the pre-existing bands leftover from the cold-work, on account of the obstacle strength of the dislocation loops already being well exceeded.

It seems very likely, meanwhile, that the interaction of the dislocation channels with grain boundaries would cause local damage by shear displacements and/or stress/strain concentrations. This would be as a result of the dislocations generated at one source boundary being deposited at the site where the channel ends, at the other boundary. Such locations could then become potential crack nucleation sites, promoting fracture along grain boundaries [19]. Indeed, Toivonen et al. observed thin, regularly-spaced slip lines emerging at the grain-boundary surface of the intergranular fractures of a highly-irradiated 304 stainless steel following room temperature tensile testing [3]. In studying proton-irradiated materials, Jiao and Was quantified the steps formed at the bar surface of materials deformed in an argon environment. Intergranular crack initiation was observed in such specimens when tested in BWR environment, and they also associated the cracking to strain localization impinging on the grain boundaries [20].

The extent of softening following yield has significant implications from the standpoint of crack propagation and crack tip plasticity. In cases where significant strain hardening capacity remains, or even that significant elongation must occur before the onset of strain softening, there is a possibility that an initiated crack could still arrest. In the case of immediate, dramatic softening however, as exhibited by the irradiated cold-worked material of this study, once a crack initiates, one might see rapid propagation, with little chance for arrest.

Also, it should be considered that mechanistic models for stress corrosion cracking correlate the crack propagation rate to the straining rate or stress concentration at the crack tip. When the plastic deformation in the crack tip zone occurs in a homogeneous way (as is the case with materials exhibiting strain hardening), the crack tip strain rate and stress is limited by the distribution of stress and strain in the zone ahead of the crack tip. However, when strain localization by dislocation channelling occurs, the stresses and strains are concentrated in very narrow zones, where the channels intersect with the grain-boundary. Finite element analysis of the effect of strain localization on the stress and strain distributions at the intersection between bands and grain boundaries have shown that the strain localization causes strong amplification of the local stresses and strains, when compared to a material with the same yield stress, deforming in a homogeneous way. These calculations have been described in detail by Sauzay et al. [21]. Thus, irradiation hardening is potentially far more damaging than hardening by cold-work, shown experimentally in [22].

5. Conclusions

The purpose of this study was to examine the deformation behaviour and mechanisms of a cold-worked AISI 304 austenitic stainless steel following irradiation. The study examined the effect of up to 3.85 dpa neutron irradiation on the deformation behaviour and microstructures of material tensile tested at room temperature and 300 °C, resulting in the following conclusions:

- The deformation behaviour of 0.07 dpa material was similar to that of non-irradiated material tested at the same temperature, showing significant strain hardening capacity, but the irradiated material's stress–strain curve was shifted upwards by about 200 MPa with respect to the non-irradiated material.
- The materials irradiated to greater levels were hardened an additional 200–300 MPa over that of the 0.07 dpa material, but they all showed an extremely limited capacity for additional work hardening, mostly exhibiting continuous softening with further straining beyond the yield point, on account of strain localization to shear bands.
- In comparison to annealed 304 material, at the lower dose level the hardening by cold-work was as significant as the increase in hardness occurring as a consequence of irradiation. At higher dose, however, the yield strength of cold-worked material was

about 400 MPa higher than that of material irradiated in the annealed condition, but while the cold-worked material continuously softened immediately following the yield peak, the high dose annealed material showed a significant delay before the onset of further softening.
– The observed behaviour is most likely a consequence of planar deformation products induced during the prior cold-work, serving as strengtheners to the unirradiated bulk on the one hand, while promoting strain localization on the other. That strain localization would then be exacerbated by the subsequent neutron irradiation.

Acknowledgment

The authors thank the European project PERFECT for financial support (Contract No. F160-CT-2003-508840).

References

[1] M.P. Manahan, R. Kohli, J. Santucci, P. Sipush, Nucl. Eng. Des. 113 (1989) 297.
[2] T. Onchi, K. Hide, M.L. Castaño, M. Navas, A role of localized plastic deformation on intergranular crack initiation of irradiated, thermally sensitized type 304 stainless steels in inert gas and in water, in: Proceedings of 10th International Conference on Environmental Degradation of Materials in Nuclear Power Systems-Water Reactors, NACE, 2001, # 67.
[3] A. Toivonen, U. Ehrnstén, W. Karlsen, P. Aaltonen, J.-P. Massoud, J.-M. Boursier, Fractographic observations on a highly irradiated AISI 304 steel after constant load tests in simulated PWR water and argon and after supplementary tensile and impact tests, in: Proceedings of 12th International Conference on Environmental Degradation of Materials in Nuclear Power Systems-Water Reactors, NACE, 2005, pp. 327–336.
[4] Z. Lu, T. Shoji, Y. Takeda, Y. Ito, A. Kai, S. Yamazaki, Corros. Sci. 50 (2008) 561–575.
[5] S.M. Bruemmer, E.P. Simonen, P.M. Scott, P.L. Andresen, G.S. Was, J.L. Nelson, J. Nucl. Mater. 274 (1999) 299–314.
[6] J.E. Pawel, A.F. Rowcliffe, D.J. Alexander, M.L. Grossbeck, K. Shiba, J. Nucl. Mater. 239 (1996) 126–131.
[7] J. Nagakawa, K. Ueno, Y. Murase, N. Yamamoto, J. Nucl. Mater. 367–370 (2007) 910–914.
[8] C. Pokor, Y. Brechet, P. Dubuisson, J.-P. Massoud, X. Averty, J. Nucl. Mater. 326 (2004) 30–37.
[9] J.W. Brooks, M.H. Loretto, R.E. Smallman, Acta Metall. 27 (1979) 1839–1847.
[10] E.H. Lee, M.H. Yoo, T.S. Byun, J.D. Hunn, K. Farrell, L.K. Mansur, Acta Mater. 49 (16) (2001) 3277–3287.
[11] J. Gittus, Irradiation Effects in Crystalline Solids, Applied Science Publisher, London, 1978.
[12] D.J. Edwards, E.P. Simonen, S.M. Bruemmer, J. Nucl. Mater. 317 (2003) 13–31.
[13] T. Onchi, K. Dohi, N. Soneda, M. Navas, M.L. Castaño, J. Nucl. Mater. 320 (3) (2003) 194–208.
[14] PRIS project data, confidential.
[15] N. Hashimoto, T.S. Byun, K. Farrell, J. Nucl. Mater. 351 (1–3) (2006) 295–302.
[16] W. Karlsen, K. Dohi, T. Onchi, Observations of channel deformation in mildly-deformed, low-dose 304L austenitic stainless steel, in: Proceedings of 13th International Conference on Environmental Degradation of Materials in Nuclear Power Systems-Water Reactors, CNS–SNC, 2007.
[17] F.A. Garner, Irradiation performance of cladding and structural steels in liquid metal reactors, Materials Science and Technology: A Comprehensive Treatment, vol. 10A, VCH Publishers, 1994, p. 419 (Chapter 6).
[18] D.J. Edwards, B.N. Singh, J.B. Bilde-Sørensen, J. Nucl. Mater. 342 (2005) 164–178.
[19] T. Onchi, K. Dohi, M. Navas, W. Karlsen, J. Nucl. Sci. Technol. 43 (8) (2006) 851–865.
[20] Z. Jiao, G.S. Was, J. Nucl. Mater. 382 (2008) 203–209.
[21] M. Sauzay, K. Bavard, W. Karlsen, J. Nucl. Mater. 406 (2010) 152–165. on PERFECT project (Special Issue).
[22] M.C. Hash, J.T. Busby, G.S. Was, in: M.R. Grossbeck, T.R. Allen, R.G. Lott, A.S. Kumar (Eds.), Proceedings of 21st International Symposium On effects of irradiation in materials, STP 1447, ASTM Int., 2004, pp. 92–104.